Soils and Foundations 2015;55(2):329–342

HOSTED BY

ELSEVIER

The Japanese Geotechnical Society

Soils and Foundations

www.sciencedirect.com
journal homepage: www.elsevier.com/locate/sandf

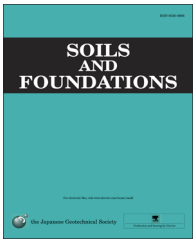

Measurement deviations for shear wave velocity of bender element test using time domain, cross-correlation, and frequency domain approaches

Toshihiro Ogino[a,*], Takayuki Kawaguchi[b], Satoshi Yamashita[b], Shunzo Kawajiri[b]

[a]*Graduate School of Engineering and Resource Science, Akita University, 1-1 Tegata-gakuen machi, Akita, Japan*
[b]*Department of Civil and Environmental Engineering, Kitami institute of Technology, 165 Koen-cho, Kitami, Japan*

Received 8 January 2014; received in revised form 30 October 2014; accepted 19 November 2014
Available online 29 March 2015

Abstract

Discrepancies in shear wave velocity measurements, attributed to the use of different methods to estimate travel time, for the bender element test were examined for various types of samples in this paper. A series of bender element tests using three different techniques, the time domain (TD), cross-correlation (CC), and frequency domain (FD) techniques, were performed to estimate travel times on identical specimens in triaxial or unconfined compression apparatuses. Experimental results revealed that the CC technique can provide reasonable values of the travel time by the maximum peak point for soft soils, while it is difficult to apply to sandy or artificially treated soils because of the unclear arrival point. From both, experimental investigation and numerical analysis of CC, the frequency dependence of the travel time is demonstrated. As a result of travel time estimation using frequency sweep signals, strong dispersion and scattering of phase and group velocities due to the non-linearity of the test system are indicated in the FD technique. The FD technique broadly underestimates the shear wave velocity compared with the TD technique, a trend shown in most soil samples. Shear wave velocities obtained from the CC and FD techniques are also compared with those obtained from the TD technique.

Keywords: Bender element test; Shear wave velocity; Time domain; Frequency domain; Cross-correlation

1. Introduction

Shear wave velocity measurement using the bender element, which was originally introduced by Shirley and Hampton (1978) and was widely spread to many researchers by Dyvik and Madshus (1985), is a practical method which came to be embedded in laboratory test apparatuses in the mid 1980s. Bender elements are well-known as low-cost and simple tools to measure the shear wave velocity of soil in a laboratory (e.g., Gu et al., 2013; Seng and Tanaka, 2012). In early use of the bender element test, the travel time of the shear wave was determined by the distance between characteristic points of the transmitted and received waveforms, and thence the shear wave velocity V_s was evaluated as

$$V_s = L/\Delta t, \tag{1}$$

where L and Δt are the travel distance and travel time of the shear wave, respectively. This approach has recently been labeled the time-domain (TD) technique. Due to the problem of the near-field effect frequently masking the characteristic point corresponding to the arrival time, the original method has been closely investigated by many researchers to increase the precision and reliability of V_s measurements (Sanchez-Salinero et al., 1986; Brignoli et al., 1996; Arroyo et al., 2003; Arulnathan et al., 1998). Consequently, a general consensus has been reached concerning the following characteristics of TD analysis: the tip-to-tip distance

*Corresponding author.
E-mail address: ogino@gipc.akita-u.ac.jp (T. Ogino).

http://dx.doi.org/10.1016/j.sandf.2015.02.009
0038-0806/

between bender elements is reasonable for the travel distance L; one cycle of a sinusoid makes reading the travel time simpler compared to a rectangular wave; the peak-to-peak distance between the transmitted and received signals has a reasonable travel time; and higher sinusoid frequency, i.e., higher travel distance to wavelength ratio L/λ, can lessen the distortion of the received waveform caused by the near-field effect. Yamashita et al. (2009) demonstrated the effect of these improvements on shear modulus evaluation and laid the foundation for the 2011 establishment of the Japanese Geotechnical Society's standard concerning the measurement of the shear wave velocity using bender elements.

Nevertheless, the fundamental problem of determining the first arrival point in a given received waveform is not entirely solved. Depending on the conditions, such as the tested soil sample dimensions, the saturation, and the stress level, the occurrence of ambiguous waves due to the near-field effect is still difficult to prevent and complicates the detection of the first shear wave arrival. The cross-correlation (CC) technique (Viggiani and Atkinson, 1995) can be considered an alternative approach even though many researchers have commented on its limitations (Viggiani and Atkinson, 1997; Santamarina and Fam, 1997; Gajo et al., 1997; Wang et al., 2007; da Fonseca et al., 2009). Airey and Mohsin (2013) re-examine the claims made by these authors and demonstrate that CC between single- and multi-cycle sine input signals and their received signals reflects a reasonable travel time, if the input frequency and characteristic point corresponding to arrival are chosen appropriately.

The frequency domain (FD) technique, an alternate method for travel time estimation based on the phase shift between the transmitted and received signals, was also introduced in the last decade (Greening and Nash, 2004). This method provides two objective criteria for travel time determination, the secant and the tangent of phase spectra, which yield two shear wave velocities called phase and group velocities, respectively. However, both velocities obtained from FD analysis have been found to be slower than those from the TD technique even when the applied frequency range is carefully chosen (Greening and Nash, 2004; da Fonseca et al., 2009; Alvarado and Coop, 2012; Styler and Howie, 2013).

This paper comprehensively re-examines the results of the bender element test based on the TD, CC, and FD techniques to understand their characteristics, particularly the frequency dependence of the V_s measurement. A series of bender element tests using these techniques are carried out on a variety of soil samples with a wide spectrum of stiffness values. In the following section, the characteristics of the CC technique are described based on both experimental and analytical investigations. CCs are identified experimentally and numerically to reveal the frequency dependence of the CC technique. This is followed by an assessment of the phase and group velocities measured by the FD technique, including identification of the cross-spectrum using frequency sweep inputs. Finally, these velocities are compared with that from the TD technique, which is based on the standard of the Japanese Geotechnical Society.

2. Laboratory equipments and experimental procedures

Ten types of soil samples with a wide range of stiffness parameters were prepared to compare the difference in travel times obtained from the TD, CC, and FD techniques on identical specimens under identical conditions. The physical properties of the samples are shown in Table 1. Appropriate preparation methods were applied for each sample: air pluvia-

Table 1
Physical properties of tested soil samples and states of specimens during V_s measurement.

Sample name	Soil particle density ρ_s(t/m^3)	Maximum void ratio e_{max}	Minimum void ratio e_{min}	Effective consolidation stress σ_c' (kPa)	Void ratios
Toyoura sand (dry)	2.65	0.98	0.62	25, 50, 100, 200, 400	0.69, 0.69, 0.69, 0.69, 0.69
Inagi sand (dry)	2.72	1.27	0.77	15, 25, 50, 100, 200	1.03, 1.01, 0.99, 0.96, 0.92
Glass bead d=2 mm (dry)	2.49	0.68	0.59	10, 50, 200	0.59, 0.59, 0.59
Glass bead d=0.4 mm (dry)	2.49	0.70	0.53	10, 50, 200	0.55, 0.55, 0.54
	Soil particle density ρ_s(t/m^3)	Liquid limit w_L(%)	Plastic limit w_p(%)	Effective consolidation stress σ_c' (kPa)	Void ratios
Pisa clay	2.77	81	25	20, 150, 450	1.64, 1.56, 1.27
NSF clay	2.73	67	35	88	1.29
Artificially treated soil (base soil)	2.56	86	36	Unconfined	—-
	Soil particle density ρ_s(t/m^3)	Ignition loss L_i(%)	Initial water content ω_0(%)	Effective consolidation stress σ_c' (kPa)	Void ratios
Ebetsu organic clay	2.34	22.4	288	17, 38	4.68, 2.93
Ebetsu peat	1.99	46.5	371	34, 55	6.76, 5.49
Akita peat	1.64	76.5	630	17–300	6.56–2.95

tion for sandy soil or glass beads, pulling out of a thin walled tube or preconsolidation cell and trimming to given dimensions for clayey or peaty soil, or curing in a mold for artificially treated soil (Kataoka et al., 2013). The dimensions of the specimens are 75 mm diameter and 150 mm height for peat and organic clay, and 50 mm diameter and 100 mm height for other samples.

Apart from the artificially treated soil, specimens are isotropically consolidated at a prescribed stress in a triaxial cell, where the transmitter and receiver elements are installed in the top cap and pedestal, respectively. At the end of primary consolidation, the bender element tests are implemented under consolidation stress. Certain measurements using single-period sinusoids and frequency sweep signals are carried out so that V_s in identical specimens can be simultaneously evaluated by the TD, CC, and FD techniques. Frequencies for single-period sinusoids were selected from the range of 1 to 100 kHz corresponding to the stiffness of each sample. For artificially treated soil specimens, the same procedures were performed under unconfined conditions in unconfined compression apparatuses. The dimensions of the bender elements are as follows: 12 mm in length (i.e., the length embedded in top cap or pedestal and soil specimen are 7 and 5 mm, respectively), 10 mm in width, and 0.5 mm in thickness. A substantial length of 5 mm was inserted into the specimen. An epoxy resin coating 0.5 mm in thickness was applied for waterproofing and insulation. The setup for the bender element test consisted of a pair of bender elements installed in triaxial or unconfined compression apparatuses, a function generator (WF1974 or WF1945, NF Corporation), and a digital oscilloscope (DS-5554, Iwatsu Test Instruments Corporation or DL1740, Yokogawa Corporation). The sampling frequencies of the function generator and the digital oscilloscope are 30 and 500 MHz, respectively. Data for the transmitted and received signals were recorded by the oscilloscope. The analysis for travel time determination with each technique was carried out after each test was finished.

Triaxial cyclic loading tests were performed on some samples after V_s measurements in order to confirm the reliability of the TD analysis. The amplitude of the axial strain was 0.005% and the number of cycles was 11.

3. Techniques of travel time estimation

3.1. Time domain technique

In the TD technique, a high value of L/λ reduces signal distortion in the received wave and simplifies the detection of the arrival time. Using the fundamental relation $Vs = f_T\lambda$ and Eq. (1), the L/λ ratio can be written as

$$L/\lambda = f_T \Delta t, \tag{2}$$

where f_T is the input signal frequency to drive the transmitter element. Given a constant Δt, L/λ can only be controlled by adjusting the frequency. In practical situations, variations in the shear wave velocity due to using different soil samples or stress levels results in major variations in the travel time Δt, if the height of the specimen is fixed. This means that a satisfactory frequency for a given value of L/λ varies across a wide spectrum of frequencies, depending on the type of soil or the applied stress level.

In this study, appropriate frequencies are found according to the Japanese Geotechnical Society's standard (Japanese Geotechnical Society, 2011), then the travel time of the shear wave is estimated: (1) for every data set, travel times Δt_{TDs} and Δt_{TDp} are evaluated by the start-to-start and peak-to-peak distances of transmitted and received waves, respectively. (2) Data with L/λ ratios less than two are excluded to prevent the near-field effect. (3) Results with errors between Δt_{TDs} and Δt_{TDp} of over 3% are excluded. (4) Finally, Δt_{TD} is given by

$$\Delta t_{TD} = \frac{\Delta t_{TDs} + \Delta t_{TDp}}{2}. \tag{3}$$

When more than two datasets are applicable, the mean value of Δt_{TD} is adopted.

3.2. Cross-correlation technique

The CC function is given by

$$cc_{xy}(\tau) = \lim_{T\to\infty} \frac{1}{T} \int_0^T x(t)\, y(t+\tau)\, dt, \tag{4}$$

where $x(t)$ and $y(t)$ are the transmitted and received signals, respectively, and T is the recording time. Eq. (4) can also be written as an alternative expression of the cross-spectrum between the transmitted and received waves in the FD

$$CC_{xy}(f) = X(f)Y(f)^*, \tag{5}$$

where $CC_{xy}(f)$, $X(f)$ and $Y(f)$ are the Fourier transforms of $cc_{xy}(\tau)$, $x(t)$ and $y(t)$, respectively, and the asterisk denotes the complex conjugate. CC's are easily given by calculating the inverse Fourier transform of $CC_{xy}(f)$ in Eq. (5). The travel time of the shear wave is defined as the time corresponding to the maximum and first peak point of CC. The former is denoted by Δt_{CC1} and the latter by Δt_{CC2}. Δt_{CC2} is manually determined from multiple signals recorded with different input frequencies, while Δt_{CC1} is automatically determined. Generally, Δt_{CC1} does not provide a reasonable travel time when sandy soil is tested (Airey and Mohsin, 2013; Yamashita et al., 2009). Δt_{CC1} and Δt_{CC2} are essentially identical when the maximum peak point is consistent with the first peak.

3.3. Frequency domain technique

When applying the FD technique to estimate the travel time, a frequency sweep signal is commonly used because of its wide frequency spectrum. The travel time is then obtained from the phase difference of the cross-spectrum between the transmitted and received waves. Two kinds of travel times, i.e., Δt_{ph} and Δt_{gr} corresponding to the phase and group velocities, respectively, can be defined by the slope of the phase spectrum. Δt_{ph}, given by the secant of the spectrum at frequency f, is described as

$$\Delta t_{ph} = -\frac{1}{2\pi}\frac{\phi}{f}, \tag{6}$$

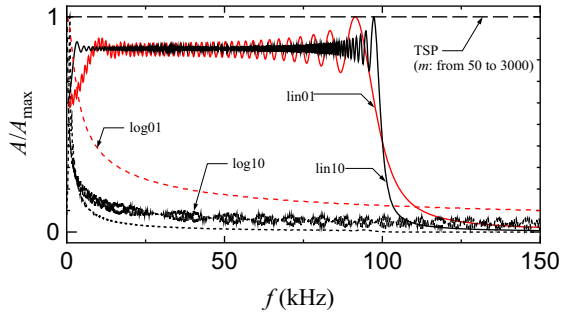

Fig. 1. Fourier spectrum of frequency swept signals.

where ϕ is the unwrapped phase of the spectrum. Δt_{gr}, defined as the tangent of the spectrum at frequency f, is given by

$$\Delta t_{gr} = -\frac{1}{2\pi}\frac{\partial \phi}{\partial f}. \tag{7}$$

Eqs. (6) and (7) indicate that Δt_{ph} requires the absolute phase shift of transmitted and received waves for estimation, while Δt_{gr} can be obtained from the relative phase shift. Offsets to the absolute phase can be evaluated by the combined identification of TD and FD analysis (Styler and Howie, 2013), with the results of TD analysis from Eq. (3), or the π-point technique (Greening and Nash, 2004).

Three types of sweep signals are used: linear sine sweep (e.g., Greening and Nash, 2004; da Fonseca et al., 2009; Styler and Howie, 2013), log sine sweep, and time-stretched pulse (TSP) (Aoshima, 1981). In discrete time, each signal can be written as follows. For linear sweep signals

$$x_{lin}(t) = \begin{cases} A \sin 2\pi\left(f_0 + \frac{t}{t_t}\Delta f\right)t, & 0 \le t \le t_t \\ 0, & t_t \le t \le N\Delta t \end{cases}$$
$$t = k\,\Delta t \quad (k = 0, 1, 2, \ldots, N)$$
$$\Delta t = f_s^{-1}, \tag{8}$$

where $x_{lin}(t)$ is the time history of the linear sweep, A is the amplitude, f_0 and Δf are the origin and width of the frequency sweep, respectively, t_t is the duration of the frequency sweep, N is the number of data points, Δt is the discrete time, and f_s is the sampling frequency. For log sweep signals

$$x_{log}(t) = \begin{cases} A \sin 2\pi\left(10^{\left(\frac{t}{t_t}\log\left(1+\frac{\Delta f}{f_0}\right)\right)} f_0\right)t, & 0 \le t \le t_t \\ 0, & t_t \le t \le N\Delta t \end{cases}$$
$$t = k\,\Delta t \quad (k = 0, 1, 2, \cdots, N)$$
$$\Delta t = f_s^{-1}, \tag{9}$$

where $x_{log}(t)$ is the time history of the log sweep. For TSP,

$$X_{TSP}(k) = \begin{cases} A \exp\left(i\frac{4m\pi k^2}{N^2}\right), & 0 \le k \le \frac{N}{2} \\ X^*(N-k), & \frac{N}{2}+1 \le k \le N \end{cases}$$
$$f(k) = \frac{k}{N\,\Delta t} \quad (k \le N/2)$$

Table 2
Values of parameters for sweep signals.

Name	Type	A(V)	f_s (kHz)	N	f_0(kHz)	Δf(kHz)	t_t (ms)	m
lin01	Linear sweep	10	10,000	10,000	0	50	1	–
lin10		10	10,000	100,000	0	50	10	–
log01	Log sweep	10	10,000	10,000	0.001	100	1	–
log10		10	10,000	100,000	0.001	100	10	–
TSP50								50
TSP100								100
TSP300								300
TSP600	TSP	1	5000	10,000	–	–	–	600
TSP1000								1000
TSP2000								2000
TSP3000								3000

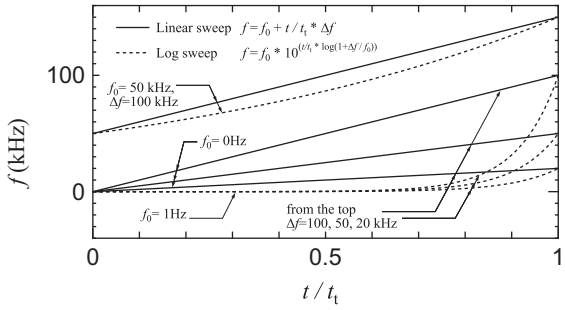

Fig. 2. Normalized time vs. frequency relationship of linear and log sine sweeps.

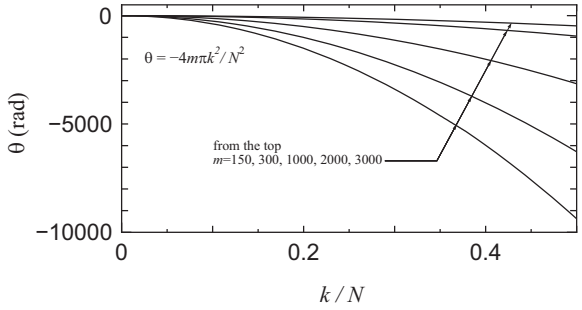

Fig. 3. Normalized frequency vs. phase relationship of TSP.

$$\Delta t = f_s^{-1}, \tag{10}$$

where $X_{TSP}(k)$ is the Fourier transform of TSP, m is a parameter relating to the degree of sweeping, and $f(k)$ is the discrete frequency. The frequency increases linearly with time in Eq. (8) and exponentially in Eq. (9), while the phase shifts are proportional to square of the frequency in Eq. (10). Fig. 1 shows the amplitudes of the Fourier spectra of the sweep signals, exhibiting remarkable amplitude decay in the high frequency range for the log sweep signals, while maintaining the amplitudes for the linear sweep and TSP signals. The

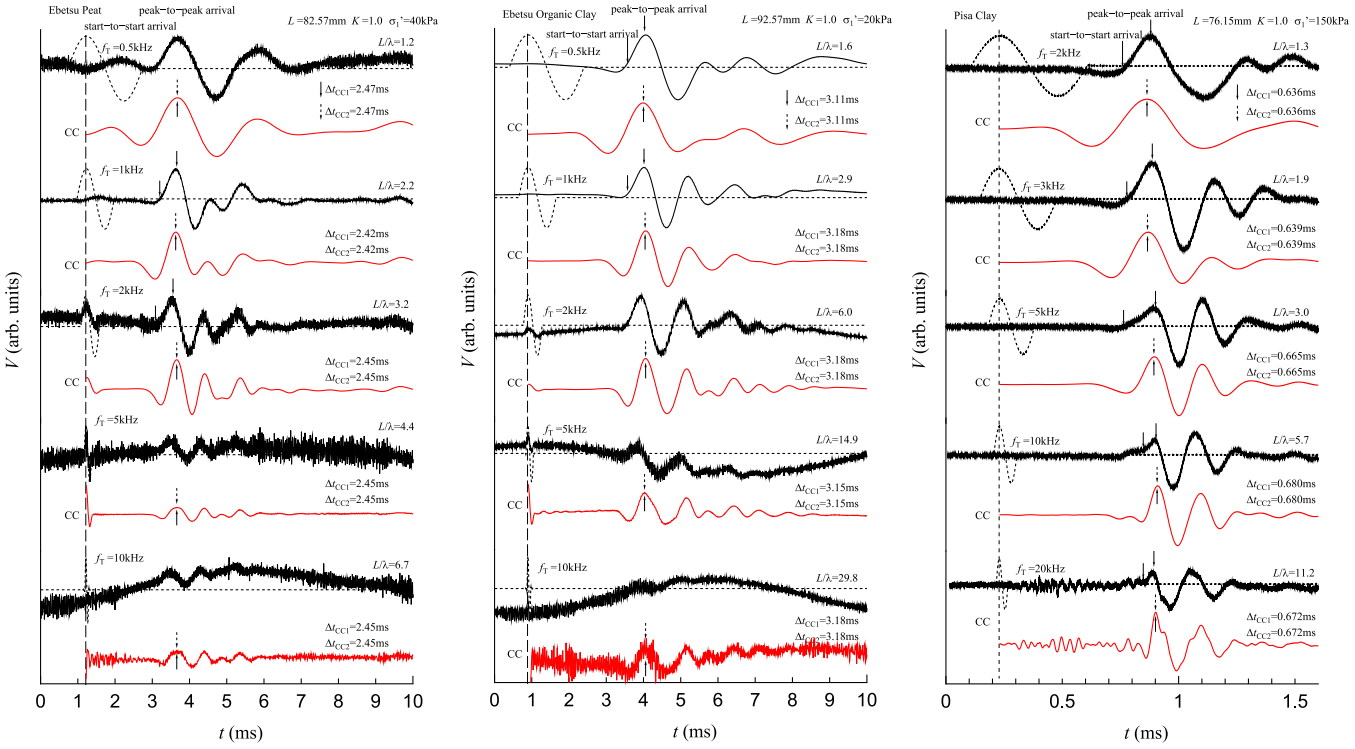

Fig. 4. Typical results of bender element test on soft soils.

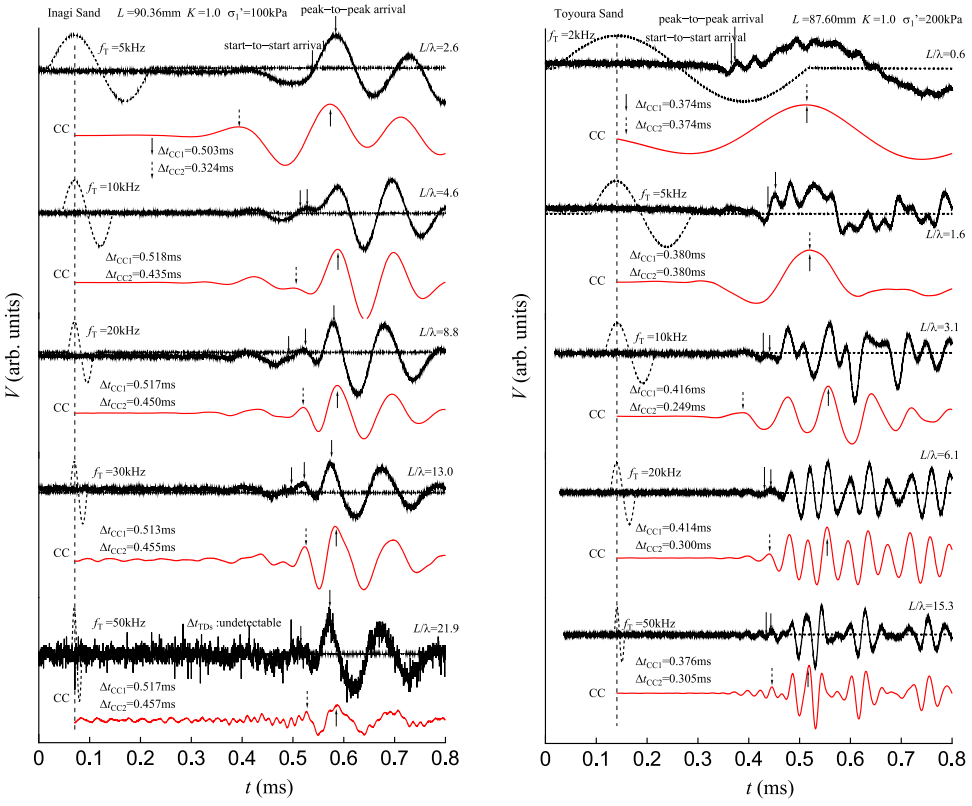

Fig. 5. Typical results of bender element test on sandy soils.

values of the parameters in Eqs. (8)– (10) are summarized in Table 2, and the frequency characteristics of the sweep signals varying with the parameters are shown in Figs. 2 and 3.

4. Results and discussion

4.1. Estimation of travel time and shear wave velocity using cross-correlation

Typical input and received waveforms of the bender element test on various soil types with a wide spectrum of input frequencies are shown in Figs. 4–6. Results that do not fulfill the criteria for travel time estimation in the TD (Section 3.1) are also represented here. Arrival points based on the start-to-start and peak-to-peak distances are represented only for fulfilled received waveforms. CC's are shown below each set of waveforms. For soft soils, waveforms of CC's show clear peak points. The first peaks are consistent with the maximum peaks, except when the input frequency is high. Travel times can be uniquely determined in accordance with the CC technique, even though the travel time Δt_{CC1} increases for Ebetsu peat (2.42–2.47 ms), Ebetsu organic clay (3.11–3.18 ms), and Pisa clay (0.636–0.680 ms).

In contrast, the maximum and first peaks do not coincide for sandy soils (Fig. 5). Similar oscillations in the beginnings of the waveforms are also observed for glass beads and artificially treated soil (Fig. 6). These oscillations are derived from ambiguous peaks observed in the beginning of the received signal. This behavior, commonly observed in sandy soils (Airey and Mohsin, 2013; Yamashita et al., 2009; Gu et al., 2013), is due to reflected P-waves and does not represent the arrival of a shear wave (Lee and Santamarina, 2005). The effect of the reflected wave is more pronounced for sandy soils than for soft soils because of long reverberations and low damping. Since the correct peak corresponding to the arrival point migrates as stress state or the travel distance varies (Airey and Mohsin, 2013), it is difficult to detect it only from the CC waveform. Considering the similarity between the CC and received waveforms, it is more direct and practical to use the peak-to-peak distance Δt_{TDp} instead of Δt_{CC2}. Note that since CC reduces signal noise (Figs. 4–6), the use of CC can be advantageous if the received wave has high noise levels.

In Figs. 7–9, shear wave velocities V_{sCC} obtained from CC are compared with velocities V_{sTD} obtained from TD analysis for various samples, with velocities fulfilling previously defined criteria (Section 3.1). Travel times for V_{sCC} estimation are determined from the maximum peak point (Δt_{CC1}). In addition to results from the observed data, the values of V_{sCC} calculated by the waveform reconstruction method (Ogino et al., 2010) are shown. These interpolate the observed data and help to clarify the relationship between the variation of V_{sCC} and the frequency variation. Values of shear moduli calculated from V_{sTD} are shown in Table 3 and compared to those obtained from other tests or well-established equations in order to confirm the reliability of TD analysis, which is in agreement with results for soft and sandy soils. The value of V_{sTD} for artificially treated soil is also reported to be consistent with PS logging results, though less than soft and sandy soils (Kataoka et al., 2013).

For soft soils and glass beads, the mean values of V_{sCC} are nearly equal to those of V_{sTD}. The discrepancy is less than 10%

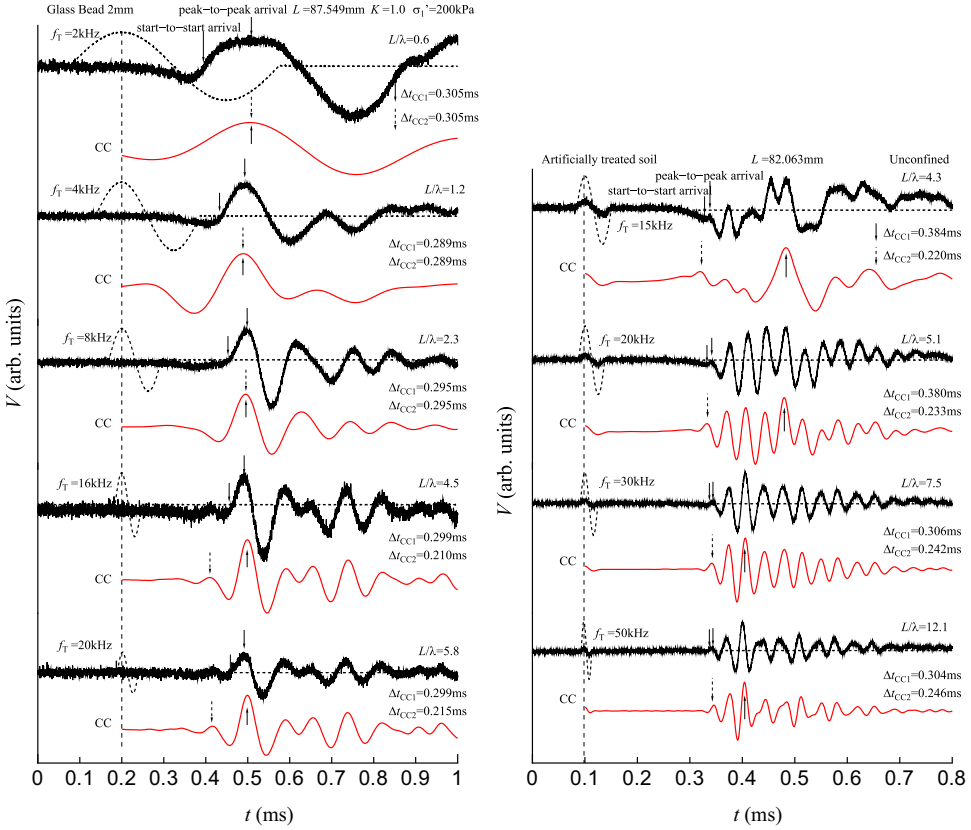

Fig. 6. Typical results of bender element test on artificially treated soil or artificial granular material.

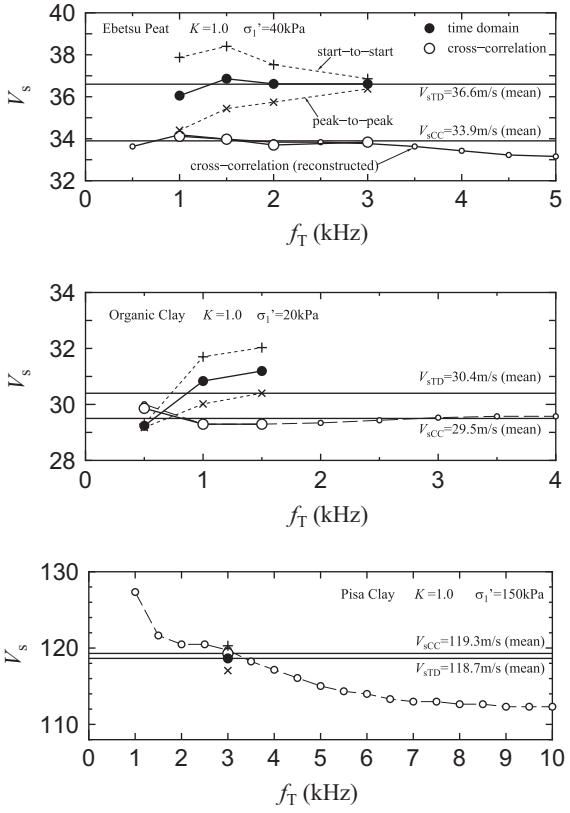

Fig. 7. Comparison of shear wave velocities obtained from time domain and cross-correlation techniques on soft soils.

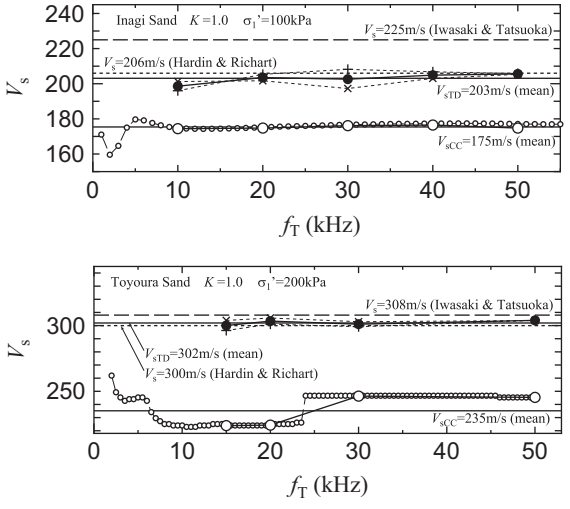

Fig. 8. Comparison of shear wave velocities obtained from time domain and cross-correlation techniques on sandy soils.

with respect to V_{sCC} and is acceptable considering the scatter of V_{sTD}. However, the difference cannot be disregarded for sandy or artificially treated soils, for which Δt_{CC1} and Δt_{CC2} do not coincide. The CC technique yields unreasonable values, significantly underestimating the shear wave velocity. Values of V_{sCC} are smaller than those from the empirical equations for Ottawa and Toyoura sands at comparable stress and void ratios (Hardin and Richart, 1963; Iwasaki and Tatsuoka, 1977).

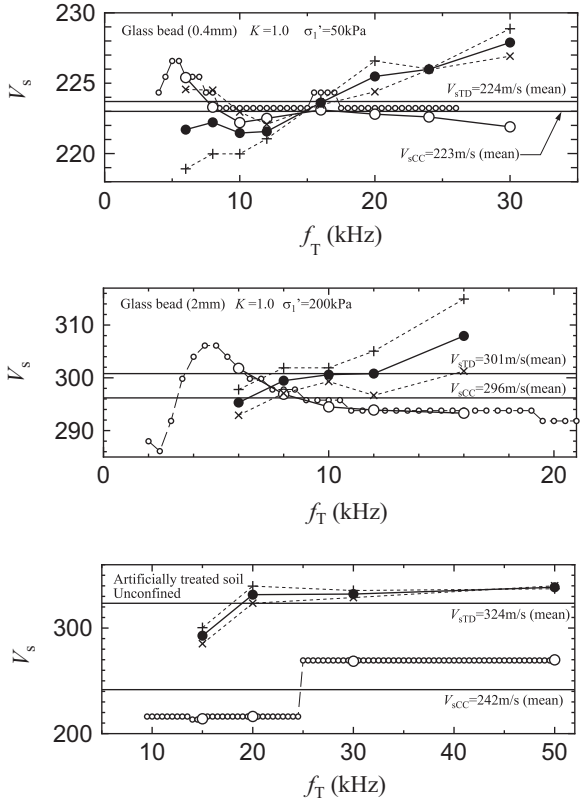

Fig. 9. Comparison of shear wave velocities obtained from time domain and cross-correlation techniques on artificially treated soil or artificial granular material.

Table 3
Comparison of shear moduli G between bender element test (TD technique) and other tests.

Sample	σ_c' (kPa)	ρ_t(t/m^3)	V_{sTD} (m/s)	G_{TD} (MPa)	G (MPa)
Ebetsu peat	34	1.15	36.6	1.54	1.56[a]
Ebetsu organic clay	17	1.24	30.4	1.14	1.14[a]
Pisa clay	150	1.69	118	23.8	20.4[a]
Toyoura sand	200	1.56	302	143	149[b]

[a]Values of G are obtained from cyclic loading test.
[b]Value of G is obtained from empirical equation by Iwasaki and Tatsuoka (1977).

Moreover, a discontinuity in the shear wave velocity can be seen at 25 kHz for Toyoura sand and artificially treated soil due to a jump of the maximum peak to the next peak as the frequency of transmitted signal varies. This means that the CC technique does not work as an alternative to the TD technique, at least for relatively stiff samples. CC analysis is effective only when the first peak of CC is consistent with the maximum peak, as with clayey or peaty soil.

4.2. Correlation of travel time in cross-correlation and time domain techniques

Although the peak of CC provides a travel time close to the TD estimation when the maximum and first peaks coincide, most of mean values of V_{sCC} are smaller than those of V_{sTD} (Figs. 7–9). Moreover, the behavior of the observed and

calculated data of V_{sCC}, which slightly decreases as frequency increases, differs from that of V_{sTD} obtained from peak-to-peak estimation. Numerical simulation using an oscillation model can provide helpful information about the behavior of the input and received signals of the bender element test. This simulation can qualitatively evaluate the position of the peak of CC and hence the frequency dependence of CC analysis. Employing a damped free vibration given by Eq. (11) as the transfer function of the receiver bender element, the received signal $y(t)$ is described by Eq. (12) (Viggiani and Atkinson, 1997; Wang et al., 2007; Styler and Howie, 2013).

$$h_r(t) = \frac{\exp(-2\pi f_n h t)}{2\pi m f_n \sqrt{1-h^2}} \sin 2\pi f_n \sqrt{1-h^2}\, t, \tag{11}$$

$$y(t) = \mathrm{IFFT}[\mathrm{FFT}[x(t)] \cdot H_s(f) \cdot \mathrm{FFT}[h_r(t)]], \tag{12}$$

where f_n is the natural frequency, h is the damping ratio, m is the system mass, $x(t)$ is the input signal, $H_s(f)$ is the transfer function of soil tested, and FFT and IFFT represent the Fourier and inverse transforms, respectively. Values of f_n and h are configured so that spectrum of $y(t)$ matches that of the observed received signal. Spectrum matching, with f_n=1 kHz and h=0.2 for Ebetsu peat (Fig. 4), can be seen to reproduce observed waveforms (Fig. 10). Predominant frequencies f_R can be determined as the peaks of the spectra (represented by arrows). Values of f_R stay at 1 kHz, equal to f_n, while f_T varies dramatically. Note that the near-field effect and waves reflected at boundaries are not considered here for simplicity, hence $H_s(f)=1$ and $m=1$ are adopted. Single-cycle sinusoids $x(t)$ yield received signals $y(t)$ (Fig. 11). So that its start position is consistent with that of the observed received waveforms (Fig. 4), $y(t)$ is rotated by 2.25 ms. Every received signal exhibits a maximum at the first peak. Δt_{TDp} can be easily estimated by the distance between the peaks in $x(t)$ and $y(t)$. CC and hence Δt_{CC1} are also yielded by Eq. (5).

Fig. 12 shows the variation in Δt_{CC1} and Δt_{TDp} with frequency compared with observed data. Frequency f_T is normalized with respect to f_R. Δt_{CC1} and Δt_{TDp} exhibit frequency dependence, but are in agreement at $f_T/f_R=1$, where the predominant frequencies of the transmitted and received signals coincide. Δt_{CC1} is greater than Δt_{TDp} in the range of $f_T/f_R>1$. The simulation results are roughly reproduced by the observed data. Fig. 13 shows the difference between Δt_{CC1} and Δt_{TD} normalized with respect to the predominant period of the received signal $1/f_R$. The model shows that the difference $\Delta t_{CC1}-\Delta t_{TD}$ is generally greater than zero and reaches a maximum of approximately 0.15, regardless of the value of f_n, and the observed data support this. Therefore, the CC technique usage involves overestimation of the travel time compared to the TD technique. As the resulting error depends on the overall travel time, it is more obvious when the predominant period is large or when the overall travel time is small. Therefore, the error may be neglected when tests are performed with a short travel distance, such as in oedometer and direct shear tests, or involve the use of extremely soft soil, such as highly organic soil.

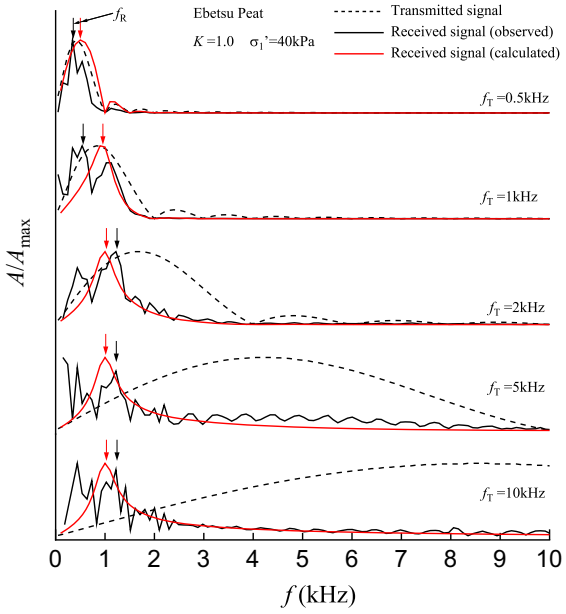

Fig. 10. Frequency characteristics of transmitted and received waves.

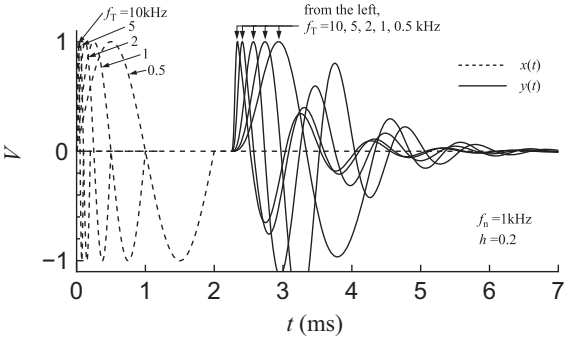

Fig. 11. Proposed model of transmitted and received waveforms.

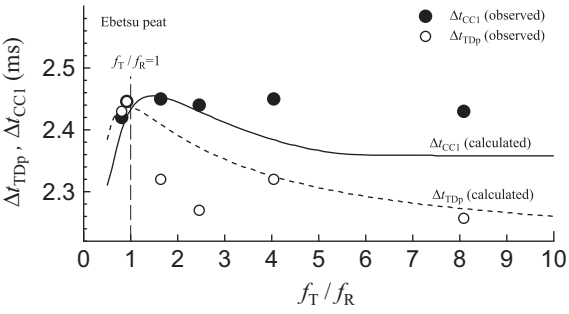

Fig. 12. Variation of travel time with frequency of transmitted wave.

4.3. Estimation of travel time and shear wave velocity using frequency domain technique

Typical waveforms of sweep inputs and the resulting received signals are shown in Fig. 14. As in Fig. 1, each type of sweep has different frequency characteristics and waveforms. Figs. 15–17 show a variety of unwrapped phase angles of cross-spectra between the two signals and their coherence functions within 20 or 50 kHz for various samples. Note that each position of the

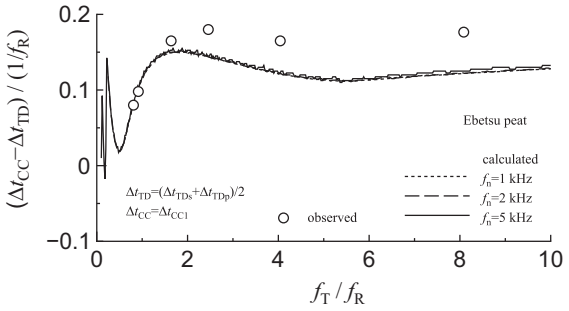

Fig. 13. Difference in travel times of time domain and cross-correlation techniques.

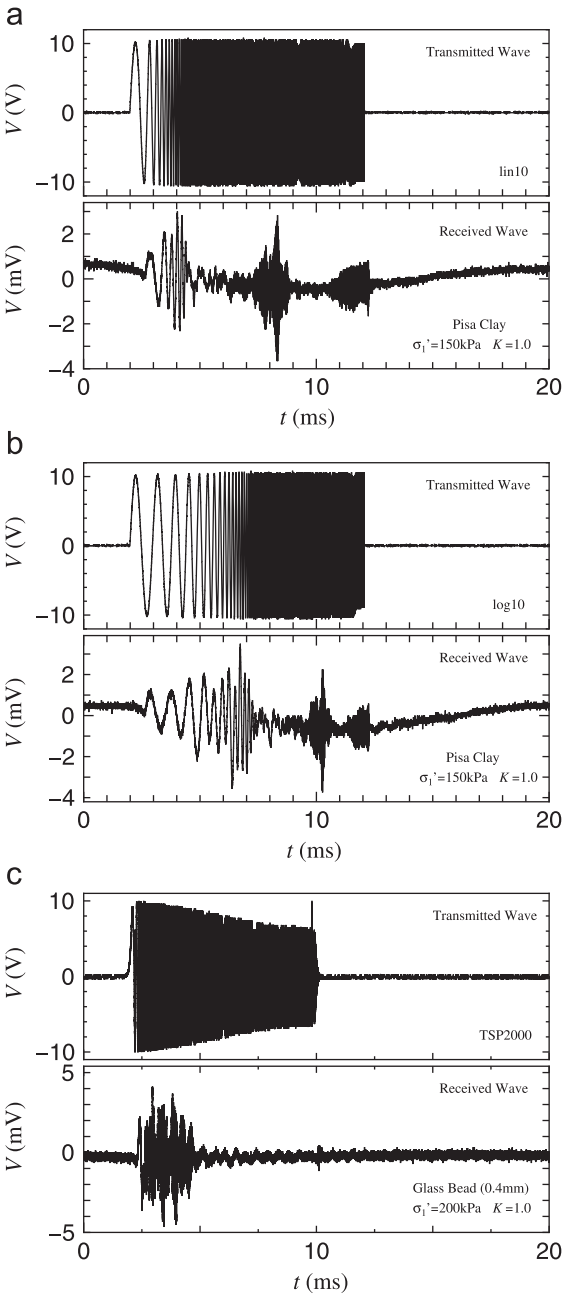

Fig. 14. Typical waveforms of frequency swept signals: (a) linear sweep, (b) log sweep, and (c) TSP.

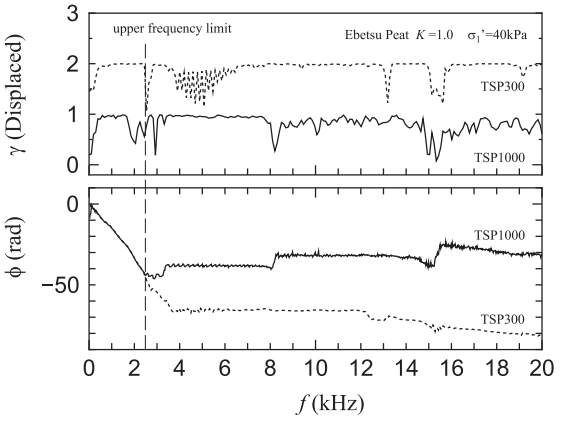

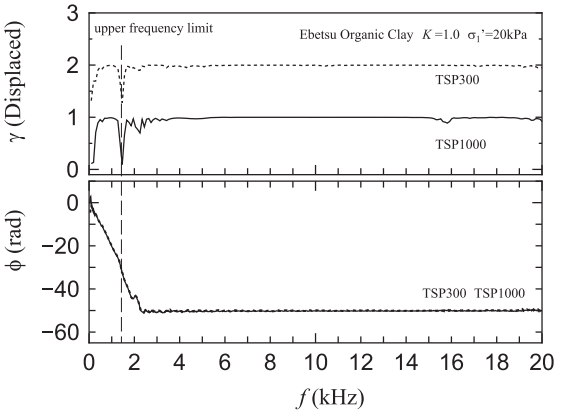

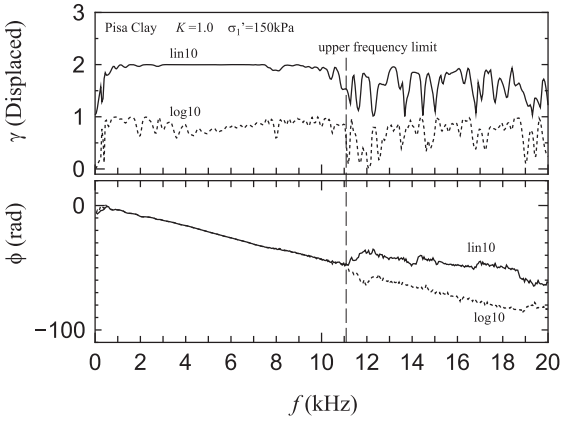

Fig. 15. Coherence γ and phase angle ϕ of cross-spectra of sweep input and received signals for soft soils.

phase spectrum is corrected by a combined TD and FD method based on previous research (Styler and Howie, 2013). The phase spectra yield travel times Δt_{ph} and Δt_{gr} as Eqs. (6) and (7). The use of the coherence function simplifies travel time estimation in the FD analysis. Styler and Howie (2013) and Fonseca et al. (2009) demonstrate that a reasonable frequency range for Δt_{ph} and Δt_{gr} estimation is associated with the range with a high coherence value. The upper frequency limit of the reasonable range is determined by a marked drop in coherence (Figs. 15–17), even though the following difficulties are found: in artificially treated soil, high coherence can be found between 25 and 40 kHz, and the phase angle shows unreasonable behavior despite the

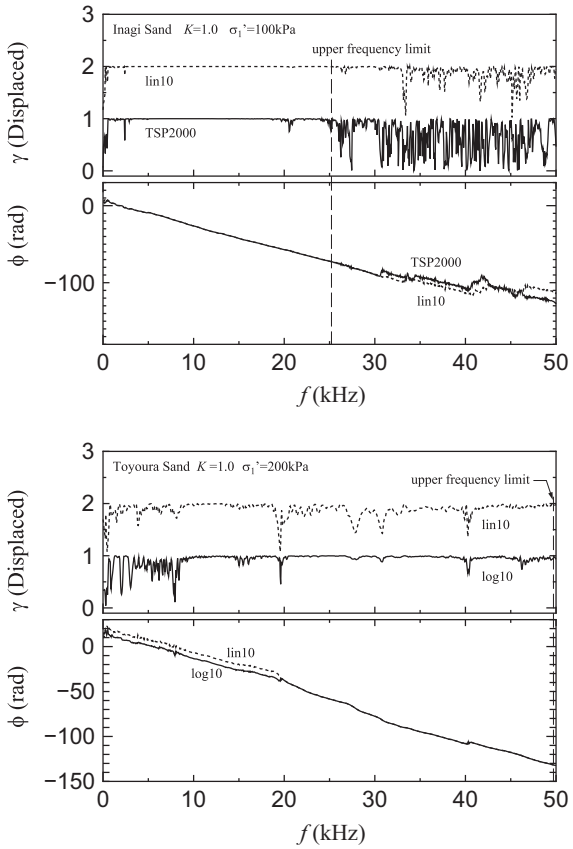

Fig. 16. Coherence γ and phase angle ϕ of cross-spectra of sweep input and received signals for sandy soils.

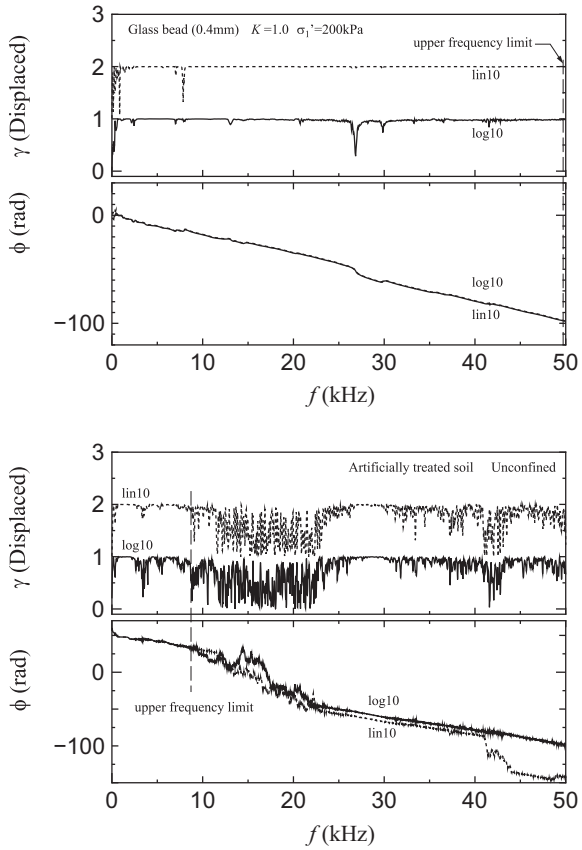

Fig. 17. Coherence γ and phase angle ϕ of cross-spectra of sweep input and received signals for artificially treated soil or artificial granular material.

high coherence range in soft soils. The phase angles exhibit a higher linearity (or less dispersion) below the frequency limit than in the range above it and are hardly affected by the input sweep signal type, despite the difference in frequency characteristics. Moreover, the location of the upper frequency limit varies dramatically with the soil sample. The values are relatively low in soft soils and over 20 kHz for sandy soil or artificial granular samples. This likely reflects the frequency characteristics of impedance between input signals and transmitter elements, or between transmitter elements and media. Given that the FD technique using a frequency sweep is essentially equivalent to identifying the transfer function, it is quite reasonable that the cross-spectrum and its coherence strongly reflect characteristics of the transfer function.

Figs. 18–20 illustrate variation in the phase velocity V_{ph} in different soil samples. The phase velocity exhibits significant frequency dependence (or strong dispersion) in all samples. The effects of the dispersion, which is attributed to soil medium-bender element coupling and the apparatus geometry, are not negligible. In particular, V_{ph} is sensitive to variations in the phase angle in the low frequency range. The significant scattering then reduces and stabilizes toward the upper frequency limit, except with artificially treated soil. Consequently, the steady values of V_{ph} at the upper frequency limit are nearly equal to values of V_{TD} for all soil samples, except artificially treated soil. The effect of input sweep type is negligible. Since the discrepancy is small, it could be acceptable for Pisa clay or Inagi sand; however, it is unacceptable for Toyoura sand. Moreover, the estimate of V_{ph} is not realistic for artificially treated soil. Taking into account the correspondence between results of the TD technique and other tests (Table 3), V_{ph} is likely to underestimate the shear wave velocity, and thence the stiffness of soils.

Similar results are yielded for group velocity V_{gr}. Figs. 21–23 show variation in V_{gr} and are comparable to Figs. 18–20. As with the phase velocity, the group velocity is widely scattered from V_{sTD}, whereas the type of sweep signal negligibly affects the frequency–velocity relationship. The values of V_{gr} within the upper frequency limit are generally below the value of V_{sTD}, indicating that V_{gr} also tends to be underestimated compared to that of V_{sTD}, even though the scattering due to dispersion is considerable. Scattering of V_{gr} from V_{sTD} is less pronounced in soft soils, indicating that the dispersion effect is likely a serious problem in relatively stiff samples. The scattering can be improved by choosing a wider fitting range to estimate the tangent of the phase spectrum (Fonseca et al., 2009). The slope of the fitted line approaches the travel time that derives the mean value of the group velocity for the overall frequency range, as the fitting range is expanded. If the system is ideal and non-dispersive, the group velocity, which is obtained from the phase spectrum making a straight line passing through the origin, is constant

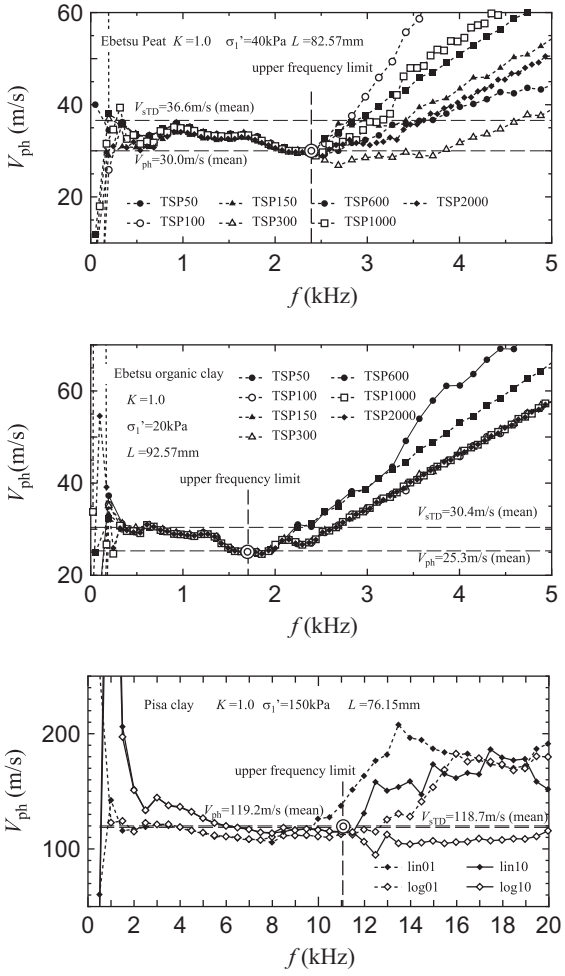

Fig. 18. Frequency dependence of phase velocity V_{ph} for soft soils.

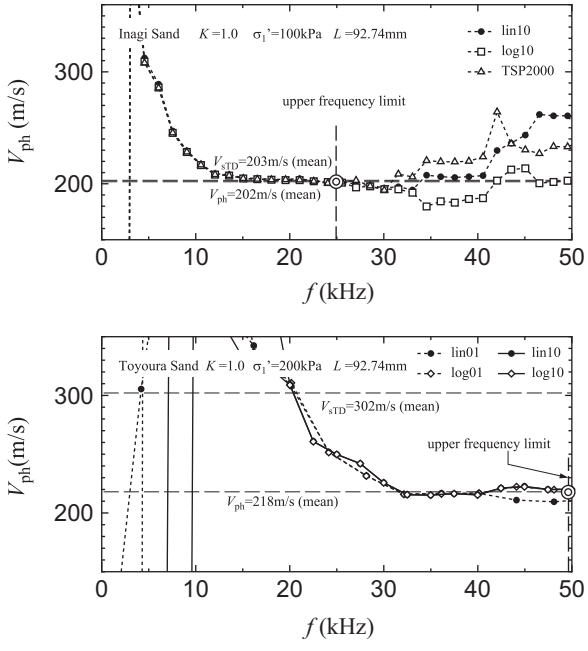

Fig. 19. Frequency dependence of phase velocity V_{ph} for sandy soils.

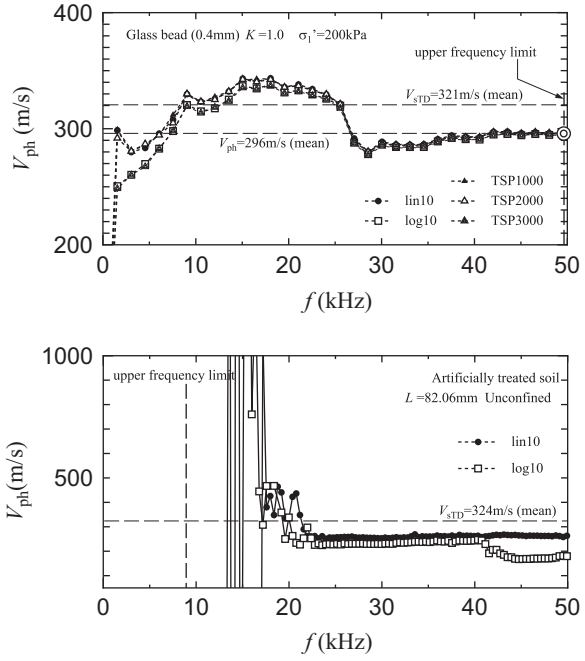

Fig. 20. Frequency dependence of phase velocity V_{ph} for artificially treated soil or artificial granular material.

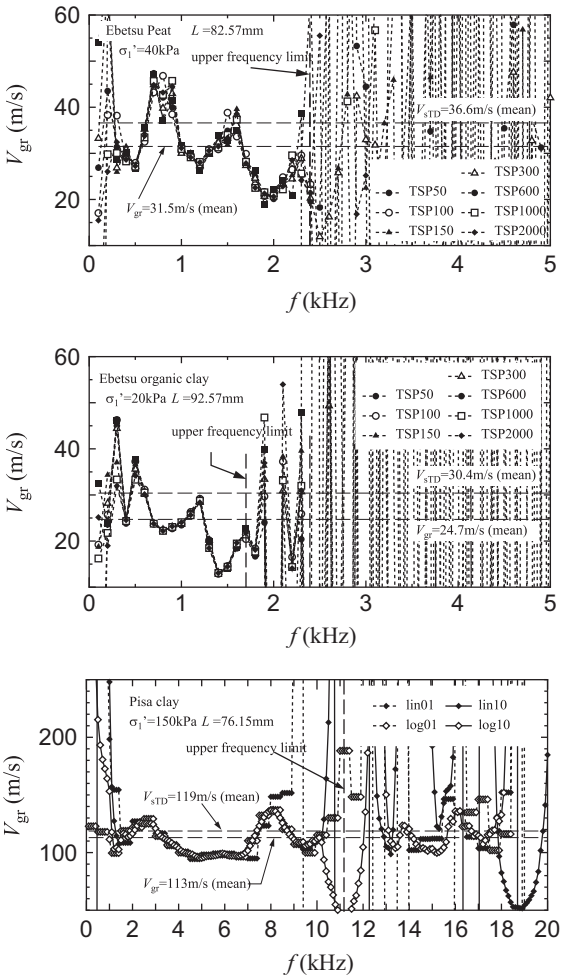

Fig. 21. Variation of group velocity V_{gr} for soft soils.

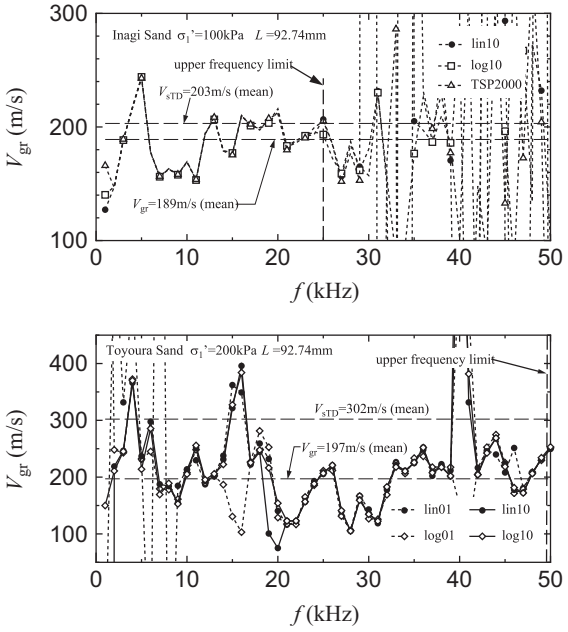

Fig. 22. Variation of group velocity V_{gr} for sandy soils.

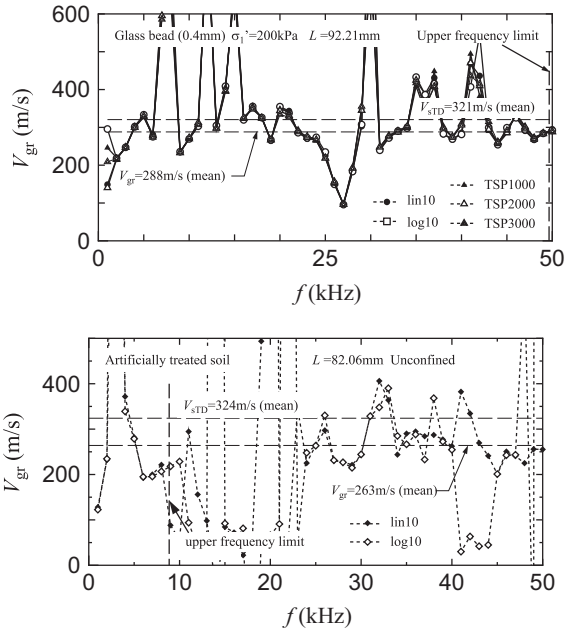

Fig. 23. Variation of group velocity V_{gr} for artificially treated soil or artificial granular material.

and equal to the phase velocity. Mean values of V_{gr} obtained from the best fit of the overall frequency range below the upper frequency limit are represented in Figs. 21–23 and summarized in Table 4. The values are stably smaller than those from the TD technique and close to those of V_{ph}. The discrepancy between V_{ph} and V_{gr} is up to 11%. This implies that the FD technique is still helpful in travel time estimation for most soil samples if the upper frequency limit is appropriately determined, even if it alone cannot provide a reasonable value.

4.4. Comparison of shear wave velocities determined by various techniques

The results of V_s measurements obtained from the CC technique are compared with those from the TD technique (Fig. 24). Travel time estimation for V_{sCC} is based on the maximum peak point in CC. Overall, data are plotted below the solid line of $V_{sCC} = V_{sTD}$, indicating that the CC technique estimates the shear wave velocity as slightly lower than the TD technique. While the discrepancy is less than 10% for soft soils, it exceeds 10%, and in some cases 20% for sandy and artificially treated soils. This is due to inconsistencies between the first and maximum peaks, and implies that if the maximum peak appears after the first peak point, this leads to significant underestimation of the shear wave velocity in these soils. As a result of the linear regression analysis applied to the data, the following relationship between V_{sTD} and V_{sCC} is derived:

$$V_{sCC} = 0.836 V_{sTD}^{\ 1.03} \tag{13}$$

The data of V_{sCC} corrected by applying the first peak of CC is also shown in the figure, suggesting the validity of the CC technique for these samples, even though it involves the same difficulty in detecting the arrival point as the TD analysis.

Figs. 25 and 26 compare shear wave velocities determined by the TD and FD techniques, showing the phase and group velocities, respectively. The V_{ph} and V_{gr} data show a trend: the FD technique estimates the shear wave velocity to be lower than the TD technique. The discrepancy is up to 20%, with some outlying samples exhibiting considerable dispersion. If these data are excluded, the best fits of V_{ph} and V_{gr} are given as follows:

$$V_{ph} = 0.885 V_{sTD}^{\ 1.01} \tag{14}$$

$$V_{gr} = 0.733 V_{sTD}^{\ 1.04} \tag{15}$$

5. Conclusions

In order to examine the discrepancies in the shear wave velocity measurements caused by different methods to estimate the travel time, a series of bender element tests using the TD, CC, and FD techniques were performed on various soil samples. From the results for 10 types of samples having wide spectrum of stiffness values, the following comprehensive conclusions were obtained.

The CCs between single sine inputs and the resulting received signals were divided into two types in accordance with the location of the maximum peak point, i.e., whether it was consistent with the first peak or not. In cases where these peaks were consistent, mainly with relatively soft soils, the CC technique provided reasonable travel times. The maximum peak of CC tended to underestimate the shear wave velocity otherwise. The first peak point, the detection of which requires manual judgment, delivered reasonable results in these cases. Thus, the CC technique can work effectively only when the maximum and first peaks coincide.

Table 4
Summary of mean values of shear wave velocities (m/s).

Sample	Ebetsu peat	Akita peat	Ebetsu organic clay	Pisa clay	NSF clay	Inagi sand	Toyoura sand	Glass bead 0.4 mm	Glass bead 2 mm	Artificially treated soil
Consolidation stress (kPa)	40	60	20	150	100	100	200	200	200	Unconfined
V_{sTD}	36.6	54.0	30.4	119	80.3	203	302	321	301	324
V_{sCC}	33.9	50.8	29.5	119	77.2	175	235	314	296	242
V_{ph}[a]	30.0	48.9	25.3	119	57.1	202	218	296	285	—-
V_{gr}[b]	31.5	48.0	24.7	113	63.7	189	197	288	291	264
Discrepancy between V_{ph} and V_{gr}	4.9%	1.9%	2.5%	5.2%	10.9%	6.6%	10.1%	2.7%	2.9%	—-

[a] V_{ph} is estimated at the upper frequency limit.
[b] V_{gr} is estimated by the best fit of the whole range below the upper frequency limit.

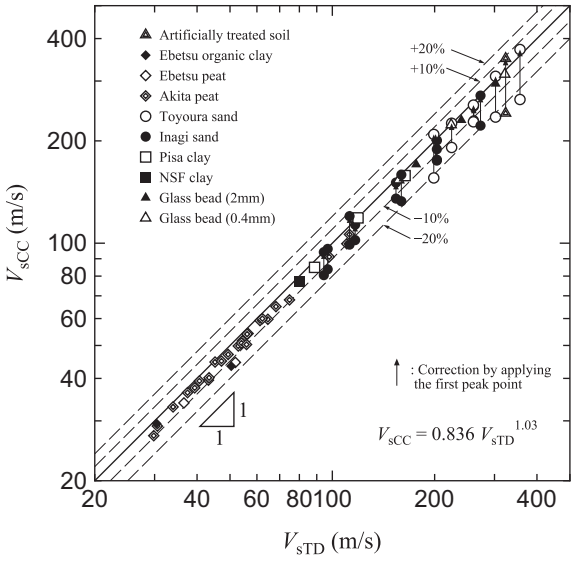

Fig. 24. Comparison of V_{sTD} and V_{sCC}.

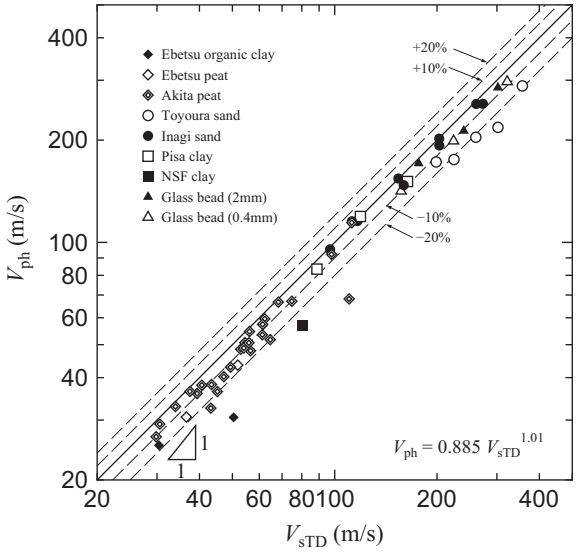

Fig. 25. Comparison of V_{sTD} and V_{ph}.

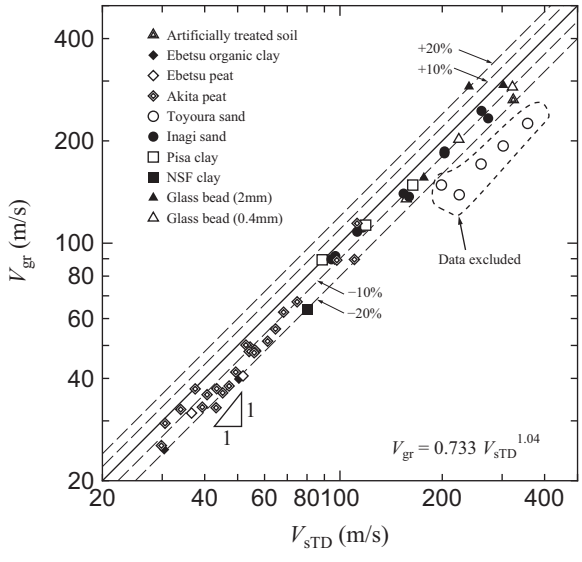

Fig. 26. Comparison of V_{sTD} and V_{gr}.

As a result of detailed examination using a numerical oscillation model, the frequency dependence of the travel time was demonstrated for the CC and TD techniques. Although the travel time determined by the maximum peak of CC was equal to that obtained from the peak-to-peak distance in the TD, only when the frequency of the sine input signal coincided with the predominant frequency of the received signal, they were fundamentally inconsistent. The value of the travel time obtained from the CC technique was larger than that from the TD technique based on the peak-to-peak distance, when the input frequency was greater than the predominant frequency of the received signal. The discrepancy between TD and CC analysis came close to approximately 0.15 times the predominant frequency of the received signal. The applicability of the FD technique was also examined. In the FD, the unwrapped phase of the cross-spectrum between the input sweep and the resulting received signals exhibited a broadly linear relationship in a plot of phase versus frequency within the high coherence frequency range. The upper limit of the frequency range varied, mainly depending on the soil stiffness. The shape of the cross-spectrum was minimally affected by the type of input sweep signal.

Even though the phase velocities evaluated by FD analysis were dispersed because of the non-linearity of the test system, the values became steady toward the upper frequency limit for most types of soil samples. Overall, the steady value of the phase velocity agreed with the shear wave velocity given by the TD technique; however, significant discrepancies were observed for a few relatively stiff samples. The group velocity exhibited a trend of underestimation of the shear wave velocity for every type of sample. The overall trend of underestimation, especially for stiff samples remained, if the fitting range to estimate the travel time was expanded.

On the basis of statistical analysis for various types of samples, relationships among shear wave velocities obtained from the TD, CC, and FD techniques were quantitatively evaluated, the results of which are given by Eqs. (13) to (15). The CC technique underestimated the shear wave velocity by 10% or less when the first peak was adopted, and the FD technique underestimated the shear wave velocity by 20% or less in the case of both the phase and group velocities.

Acknowledgments

This research was partially supported by JSPS KAKENHI Grant no. 23760438.

References

Airey, D., Mohsin, A., 2013. Evaluation of shear wave velocity from bender elements using cross-correlation. ASTM Geotech. Test. J. 36 (4), 506–514.

Alvarado, G., Coop, M., 2012. On the performance of bender elements in triaxial tests. Géotechnique 62 (1), 1–17.

Aoshima, N., 1981. Computer-generated pulse signal applied for sound measurement. J. Acoust. Soc. Am. 69 (5), 1484–1488.

Arroyo, M., Wood, D.M., Greening, P., 2003. Source near-field effects and pulse tests in soil samples. Géotechnique 53 (3), 337–345.

Arulnathan, R., Boulanger, R.W., Riemer, M.F., 1998. Analysis of bender element tests. ASTM Geotech. Test. J. 21 (2), 120–131.

Brignoli, E., Gotti, M., Stokoe, K.H., 1996. Measurement of shear waves in laboratory specimens by means of piezoelectric transducers. ASTM Geotech. Test. J. 19 (4), 384–397.

Dyvik, R. and Madshus, C., 1985. Lab measurements of G_{max} using bender elements. Advances in the Art of Testing Soils Under Cyclic Conditions. ASCE, New York, pp. 186–196.

Fonseca, A.V., Ferreira, C., Fahey, M., 2009. A framework interpreting bender element tests, combining time-domain and frequency-domain methods. ASTM Geotech. Test. J. 32 (2), 1–17.

Gajo, A., Fedel, A., Mongiovi, L., 1997. Experimental analysis of the effects of fluid–solid coupling on the velocity of elastic waves in saturated porous media. Géotechnique 47 (5), 993–1008.

Greening, P.D., Nash, D.F., 2004. Frequency domain determination of g0 using bender elements. ASTM Geotech. Test. J. 27 (3), 288–294.

Gu, X., Yang, J., Huang, M., 2013. Laboratory measurements of small strain properties of dry sands by bender element. Soils Found. 53 (5), 735–745.

Hardin, B., Richart Jr., F., 1963. Elastic wave velocities in granular soils. J. Soil Mech. Found. Div. 89 (SM1), 33–65.

Iwasaki, T., Tatsuoka, F., 1977. Effects of grain size and grading on dynamic shear moduli of sands. Soils Found. 17 (3), 19–35.

Japanese Geotechnical Society, 2011. Method for Laboratory Measurement of Shear Wave Velocity of Soils by Bender Element Test.

Kataoka, S., Tanaka, M., Tomita, R. and Nakajima, M., 2013. Effect of the dredged soil on strength development of air-form treated lightweight soil. In: Proceedings of the 18th ICSMGE.

Lee, J.S., Santamarina, J.C., 2005. Bender elements: performance and signal interpretation. J. Geotech. Geoenviron. Eng. 131 (9), 1063–1070.

Ogino, T., Mitachi, T., Oikawa, H., Takahashi, T., Tsushima, M., 2010. Frequency response characteristics of bender element test system identified by frequency-swept signal input-influence on accuracy of received waveform reconstruction. Soils Found. 50 (5), 737–745.

Sanchez-Salinero, I., Roesset, J. and Stokoe, K., 1986. Analytical Studies of Body Wave Propagation and Attenuation. Report GR 86-15.

Santamarina, J., Fam, M., 1997. Interpretation of bender element tests (discussion). Geotechnique 47 (4), 873–875.

Seng, S., Tanaka, H., 2012. Properties of very soft clays: a study of thixotropic hardening and behavior under low consolidation pressure. Soils Found. 52 (2), 335–345.

Shirley, D.J., Hampton, L.D., 1978. Shear-wave measurements in laboratory sediments. J. Acoust. Soc. Am. 63 (2), 607–613.

Styler, M.A., Howie, J.A., 2013. Combined time and frequency domain approach to the interpretation of bender-element tests on sand. ASTM Geotech. Test. J. 36 (5), 649–659.

Viggiani, G., Atkinson, J.H., 1995. Interpretation of bender element tests. Géotechnique 45 (1), 149–154.

Viggiani, G., Atkinson, J.H., 1997. Discussion: Interpretation of bender element tests. Géotechnique 47 (4), 873–877.

Wang, Y., Lo, K., Yan, W., Dong, X., 2007. Measurement biases in the bender element test. J. Geotech. Geoenviron. Eng. 133 (5), 564–574.

Yamashita, S., Kawaguchi, T., Nakata, Y., Mikami, T., Fujiwara, T., Shibuya, S., 2009. Interpretation of international parallel test on the measurement of G_{max} using bender elements. Soils Found. 49 (4), 631–650.